Published online 22 April 2015

Nucleic Acids Research, 2015, Vol. 43, No. 10 ***5171–5181***
doi: 10.1093/nar/gkv288

On the mechanism of RNA phosphodiester backbone cleavage in the absence of solvent

Christian Riml[1], Heidelinde Glasner[1], M. T. Rodgers[2], Ronald Micura[1] and Kathrin Breuker[1,*]

[1]Institute of Organic Chemistry and Center for Molecular Biosciences Innsbruck (CMBI), University of Innsbruck, Innrain 80–82, 6020 Innsbruck, Austria and [2]Department of Chemistry, Wayne State University, 5101 Cass Avenue, Detroit, MI 48202–3489, United States

Received December 01, 2014; Revised March 14, 2015; Accepted March 24, 2015

ABSTRACT

Ribonucleic acid (RNA) modifications play an important role in the regulation of gene expression and the development of RNA-based therapeutics, but their identification, localization and relative quantitation by conventional biochemical methods can be quite challenging. As a promising alternative, mass spectrometry (MS) based approaches that involve RNA dissociation in 'top-down' strategies are currently being developed. For this purpose, it is essential to understand the dissociation mechanisms of unmodified and posttranscriptionally or synthetically modified RNA. Here, we have studied the effect of select nucleobase, ribose and backbone modifications on phosphodiester bond cleavage in collisionally activated dissociation (CAD) of positively and negatively charged RNA. We found that CAD of RNA is a stepwise reaction that is facilitated by, but does not require, the presence of positive charge. Preferred backbone cleavage next to adenosine and guanosine in CAD of $(M+nH)^{n+}$ and $(M-nH)^{n-}$ ions, respectively, is based on hydrogen bonding between nucleobase and phosphodiester moieties. Moreover, CAD of RNA involves an intermediate that is sufficiently stable to survive extension of the RNA structure and intramolecular proton redistribution according to simple Coulombic repulsion prior to backbone cleavage into *c* and *y* ions from phosphodiester bond cleavage.

INTRODUCTION

Large-scale, high-throughput sequencing studies have established that >60% of a mammalian genome is transcribed or predicted to be transcribed into ribonucleic acids (RNA), but only a surprisingly small fraction, ∼2%, is actually translated into proteins (1). The considerable scale of 2′-deoxyribonucleic acid (DNA) transcription into functional, but non-coding RNA (ncRNA) only became apparent around the turn of the century, along with the finding that many ncRNAs can be extensively modified (2–5). Ever since, research into ncRNAs has progressed at a high rate, although reliable and more generally applicable methodology for the detection and characterization of posttranscriptionally or synthetically modified RNA has yet to be developed (6–10).

Mass spectrometry (MS) holds great promise for the characterization of modified RNA (8,11–29) as it can potentially detect and localize any mass-altering posttranscriptional or synthetic modifications. The most commonly used method for the generation of fragment ions from backbone cleavage, whose mass values can be aligned as 'MS sequencing ladders' (27), is collisionally activated dissociation (CAD). In typical CAD-MS experiments, gaseous ions from electrospray ionization (ESI) (30–33) are vibrationally excited by multiple, low-energy collisions with an inert gas. This process is reasonably well understood for peptides and proteins (34,35), but far fewer studies have thus far addressed the mechanisms underlying RNA dissociation (17,18,36–41). A solid understanding of phosphodiester bond cleavage into *c* and *y* ions by CAD is, however, essential to the development of new MS-based approaches for the characterization of modified RNA, including the relative quantitation of modifications. Here, we report a mechanistic study with focus on the effect of modifications towards improving our understanding of RNA phosphodiester bond cleavage by CAD.

MATERIALS AND METHODS

Experiments were performed on a 7 T Fourier transform ion cyclotron resonance (FT-ICR) mass spectrometer (Bruker, Austria) equipped with an ESI source for $(M+nH)^{n+}$ or $(M-nH)^{n-}$ ion generation depending on the electrostatic potential applied to the emitter, and a collision cell floated with Ar gas for CAD. RNA was electrosprayed at a flow rate of 1.5 μl/min from 2 μM solutions in 9:1 H_2O/CH_3OH with 20 mM ammonium acetate as additive, and polyethylene glycol 1000 (∼1 μM) was used as an internal calibrant

*To whom correspondence should be addressed. Tel: +43 512 507 57740; Fax: +43 512 507 57799; Email: kathrin.breuker@uibk.ac.at

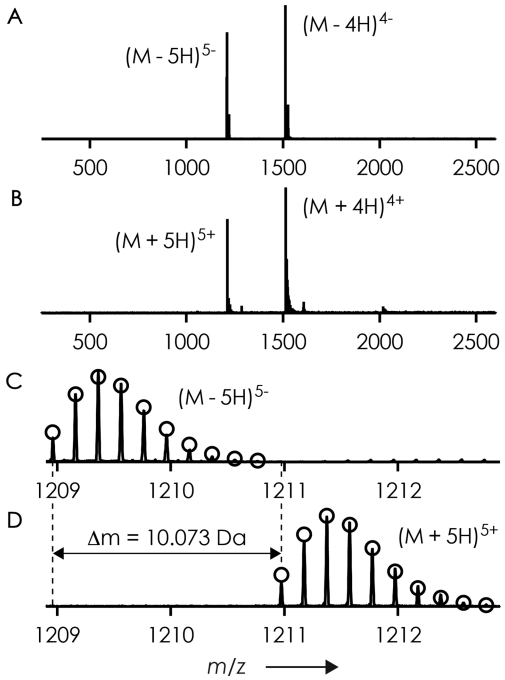

Figure 1. Mass spectra of RNA **1** (2 μM) in 9:1 H_2O/CH_3OH with 20 mM CH_3COONH_4 as additive electrosprayed in (**A**) negative and (**B**) positive ion mode; (**C**) and (**D**) show measured (lines) and calculated (circles) isotopic profiles for $(M\text{-}5H)^{5-}$ and $(M+5H)^{5+}$ ions, respectively.

for accurate mass measurements (Table 1). Methanol for ESI was HPLC grade (Acros, Vienna, Austria), H_2O was purified to 18 MΩ·cm at room temperature using a Milli-Q system (Millipore, Austria), and CH_3COONH_4 (>99.0%, Na ≤5 mg/kg, K ≤5 mg/kg) was purchased from Sigma–Aldrich (Vienna, Austria). The $(M+nH)^{n+}$ or $(M-nH)^{n-}$ ions under study were isolated by m/z in a linear quadrupole prior to dissociation in the collision cell; see (24) for a detailed description of the experimental setup for CAD. Between 25 and 100 scans were added for each spectrum, and data reduction utilized the SNAP2 algorithm (Bruker, Austria). The dinucleotide model in Scheme 3 was generated with Avogadro 2 0.7.2 software (42). Oligoribonucleotides were prepared by solid-phase synthesis using TOM chemistry (43,44), purified by HPLC, and desalted as described previously (24,27). Nucleoside phosphoramidites were obtained from ChemGenes (Wilmington, MA, USA) or Glen Research (Sterling, VA, USA). The propane-1,3-diol building block was prepared according to (45,46).

RESULTS

RNA $(M\text{-}nH)^{n-}$ and $(M+nH)^{n+}$ ions from ESI

Figure 1 shows mass spectra of RNA **1** (19 nt, see Table 1) from ESI of a 2 μM solution in 9:1 H_2O/CH_3OH with 20 mM ammonium acetate as additive in negative and positive ion mode, which gave $(M-nH)^{n-}$ and $(M+nH)^{n+}$ ions, respectively, with $n = 4$ and 5 predominating. Similar spectra were obtained for all other RNAs studied (Table 1), although n generally increased with increasing mass such that the m/z values of the majority of ions were within the range 1000–2000. Ion yields were, however, generally higher by about an order of magnitude in ESI operated in negative ion mode. To investigate the effect of ion net charge on RNA backbone cleavage, oppositely charged ions with the same absolute net charge n, $(M-nH)^{n-}$ and $(M+nH)^{n+}$, of the same RNA were each isolated in the mass spectrometer and fragmented by CAD.

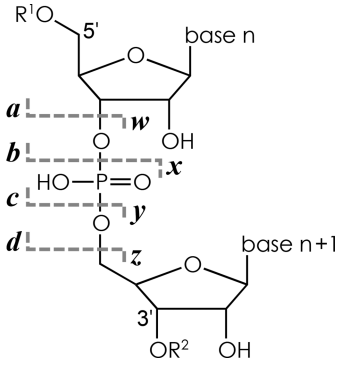

Scheme 1. Nomenclature of fragment ions from RNA backbone cleavage according to reference (48).

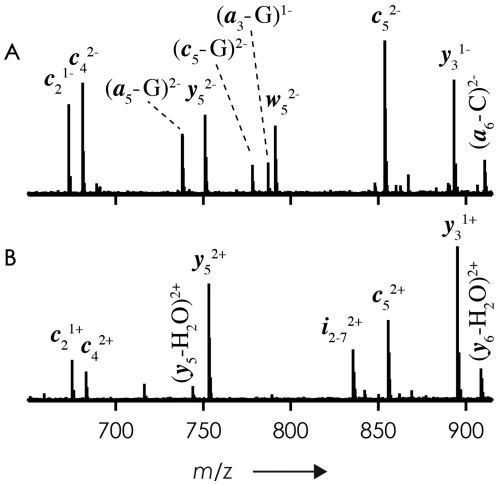

Figure 2. Segments of mass spectra from CAD of (**A**) $(M-4H)^{4-}$ and (B) $(M+4H)^{4+}$ ions from ESI of RNA **2** (2 μM solution in 9:1 H_2O/CH_3OH, 20 mM CH_3COONH_4), at laboratory frame collision energies of (A) 72 eV and (B) 44 eV.

Effect of collision energy on CAD of $(M\text{-}nH)^{n-}$ and $(M+nH)^{n+}$ RNA ions

Previous studies have shown that CAD of lowly charged $(M-nH)^{n-}$ ions of RNA (~0.2 charges/nt, 8–76 nt) produces primarily (up to 98%) (23,24) ***c***- and ***y***-type fragments from phosphodiester bond cleavage (Scheme 1) (23,24,27,39,47), and that the number of ***a***- and ***w***-type fragments from alternative $C^{3'}$–O bond cleavage increases with increasing $(M-nH)^{n-}$ ion net charge (24,39). In this study, we find that CAD of $(M+nH)^{n+}$ ions of RNA also yields predominantly ***c*** and ***y***, but virtually no ***a*** and ***w*** fragments, even at >0.2 charges/nt, as illustrated for RNA **2** (13 nt) with $n = 4$ (0.31 charges/nt) in Figure 2. Under conditions that gave ~50% ***c*** and ***y*** fragments, using 44 and 72 eV

Table 1. RNA studied

RNA	Sequence[a]	$M_{measured}$[b]	$M_{calculated}$[b]
1	CCGAA GGUUC GCCUU CGGA	6049.844	6049.835
2	GAGGG CAACC UCG	4176.630	4176.629
3	pUAAAU YUAGC UAAAA AGGGp	6297.838	6297.834
4	GGACG AUACG CGUGA AGCGU CC	7092.005	7092.010
5	GAAGG GCAAC CUUCG	4811.705	4811.707
6	GAAGG UUCGC CUUCG	4765.654	4765.653
7	GAAGG UUUUC CUUCG	4727.618	4727.615
8	GAGGU UCGCC UCG	4130.573	4130.575
9	pUAAAU GUYGC UAAA	4540.612	4540.616
10	GAGGB CBACC UCG	4130.613	4130.613
11	GAAGG DDDDC CUUCG	4223.584	4223.589
12	GAAGG PPPPC CUUCG	4055.551	4055.546
13	GAAGG RRRRC CUUCG	4287.563	4287.568
14	GAAGG aaaaC CUUCG	4875.788	4875.786

[a]from 5′ to 3′ terminus, OH-terminated unless indicated (p: phosphate); Y: 2-aminopurine, B: nebularine, P: propanediol-linker, R: ribose-spacer, D: 2′-deoxyribose-spacer, a: 2′-OCH_3 adenosine.
[b]in Da; *M* refers to monoisotopic mass.

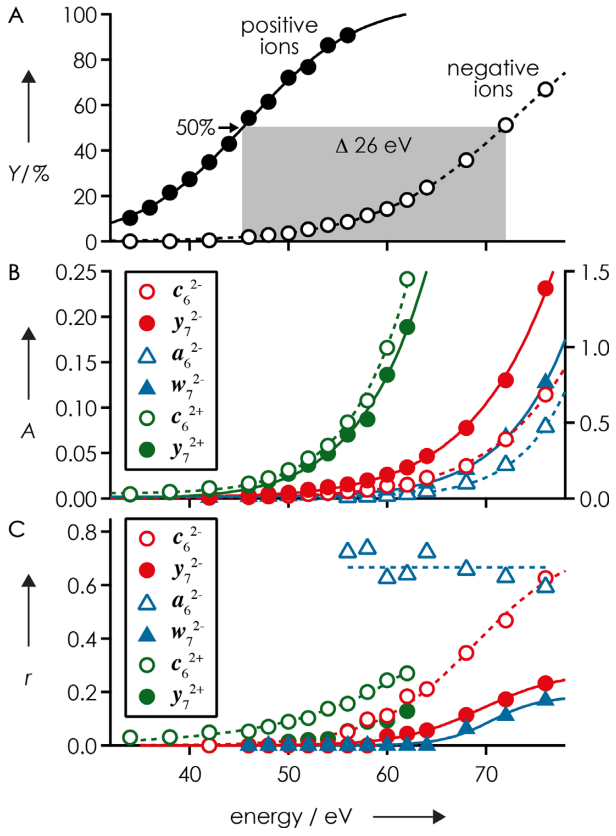

Figure 3. For RNA **2**, (**A**) yield (*Y*) of ***c*** and ***y*** fragment ions from CAD of $(M+4H)^{4+}$ (filled circles) and $(M-4H)^{4-}$ (open circles) ions, gray area highlights the 26 eV difference in energy required for 50% yield (calculated relative to ***c***, ***y***, and $(M\pm4H)^{4\pm}$ ions, considering that backbone cleavage gives a pair of complementary ***c*** and ***y*** ions, 100% = 0.5·[***c***] + 0.5·[***y***] + [$(M\pm4H)^{4\pm}$]); (**B**) fragment ion abundance *A* relative to abundance of undissociated $(M\pm4H)^{4\pm}$ ions for c_6^{2-}, y_7^{2-}, a_6^{2-}, w_7^{2-} (left axis) and c_6^{2+}, y_7^{2+} (right axis); (**C**) ratio *r* of fragment ions with and without base loss, versus laboratory frame collision energy; lines are meant to guide the eye.

(Figures 2 and 3A) for CAD of $(M+4H)^{4+}$ and $(M-4H)^{4-}$ ions, respectively, the branching ratio between ***c***, ***y*** and ***a***, ***w*** fragments was ∼3:1 for negatively and ∼30:1 for positively charged RNA **2**; similar behavior was observed for all other RNAs studied. Note that at these energies, 44 and 72 eV, the RNA ions dissociated to a similar extent, ∼75% for all $(M+4H)^{4+}$ and ∼80% for all $(M-4H)^{4-}$ ions, respectively, such that the 10-fold difference in branching ratio is primarily a result of ion polarity rather than CAD energy.

The CAD spectra in Figure 2 further illustrate H_2O loss from positively charged ***y*** fragments, and that negatively charged ***a*** fragments frequently appear as (***a*** - base) ions (39). Internal fragments from secondary backbone fragmentation (24), ***i*** ions, that do neither comprise the original 5′- or 3′-terminus, and base loss from $(M\pm nH)^{n\pm}$ ions were observed in CAD of RNA in both ion polarities. Nevertheless, ***c*** and ***y*** ions were by far the most abundant products for all RNAs and ion net charge values studied here, in either ion polarity. However, their formation by CAD generally required significantly higher energies for $(M-nH)^{n-}$ ions than for the corresponding positively charged ions, $(M+nH)^{n+}$, as shown for RNA **2** in Figure 3A. This finding is consistent with data from ion trap CAD of the RNA dinucleotide GC, whose $(M-H)^-$ ions required substantially higher excitation amplitudes for dissociation into ***c*** and ***y*** fragments than the $(M+H)^+$ ions (39).

The different energy requirements for dissociation of $(M-nH)^{n-}$ and $(M+nH)^{n+}$ ions into pairs of complementary fragments from phosphodiester bond cleavage is illustrated in more detail in Figure 3B for c_6^{2-}/y_7^{2-} and c_6^{2+}/y_7^{2+}, along with those for a_6^{2-}/w_7^{2-} ion formation (a_6^{2+}, w_7^{2+} were not observed). Although cleavage of a given backbone bond should produce the same number of complementary ***c*** and ***y***, or ***a*** and ***w*** ions, the data show that the relative abundances of negatively charged, complementary ions (c_6^{2-} and y_7^{2-} or a_6^{2-} and w_7^{2-}) differ significantly, whereas those of the positively charged c_6^{2+} and y_7^{2+} ions are more similar. This can be attributed to a lower fragment ion stability against secondary backbone cleavage and base loss from ***a***, ***c***, ***w***, and ***y*** ions at the elevated energies required for $(M-nH)^{n-}$ dissociation. Base loss was generally higher for fragments comprising the 5′ terminus (***a***, ***c*** ions), and increased with increasing energy for all fragments except for

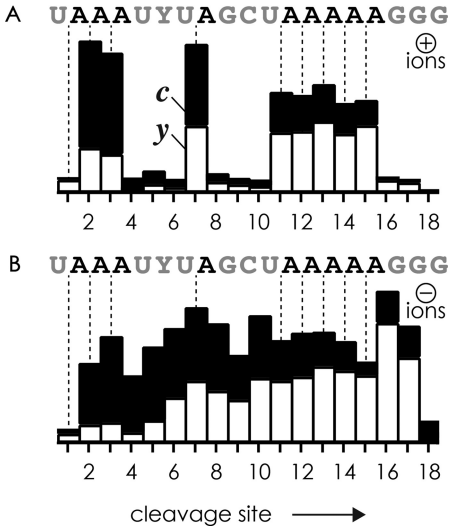

Figure 4. Relative abundances of ***c*** (black bars) and ***y*** (white bars) fragment ions from CAD of (**A**) $(M+5H)^{5+}$ and (**B**) $(M-5H)^{5-}$ ions of RNA **3** versus cleavage site, using (A) 50 eV and (B) 70 eV laboratory frame collision energies; dashed lines highlight cleavage sites on the 5′-side of adenosine residues.

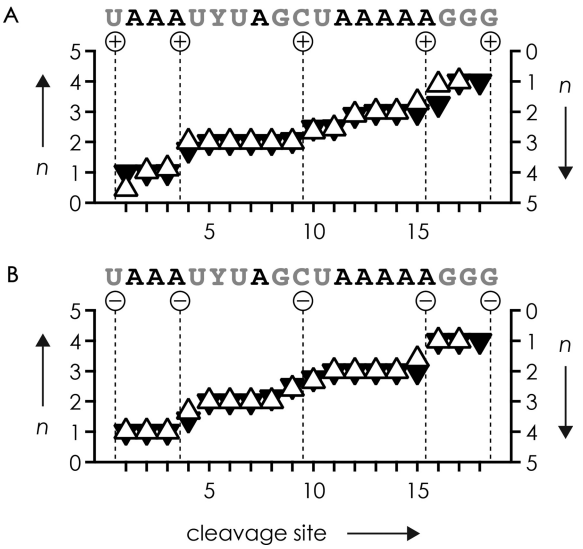

Figure 5. Average charge n of ***c*** (filled triangles, left axis) and ***y*** (open triangles, right axis) fragment ions from CAD of (**a**) $(M+5H)^{5+}$ and b) $(M-5H)^{5-}$ ions of RNA **3** versus cleavage site using (a) 50 eV and (**b**) 70 eV laboratory frame collision energy; dashed lines indicate calculated charge locations (see the supplementary material).

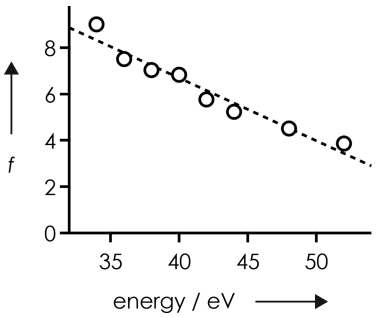

Figure 6. Average factor *f* by which backbone cleavage into ***c***, ***y*** fragments from CAD of $(M+4H)^{4+}$ ions of RNAs **2**, **5**, **6**, **7**, **8** is increased on the 5′-side of adenosine compared to other residues versus collision energy.

a ions (Figure 3C), which showed roughly the same extent of base loss at all energies used. This suggests that base loss plays a critical role only in the formation of ***a*** and ***w***, but not in phosphodiester bond cleavage into ***c*** and ***y*** ions.

The data presented thus far strongly suggest that backbone cleavage into ***a*** and ***w*** fragments involves negative charge, whereas backbone cleavage into ***c*** and ***y*** fragments can proceed in the presence of both positive and negative charge, unless ***a*** and ***w*** ion formation becomes competitive at high net negative charge (39). However, net positive charge appears to facilitate backbone cleavage into ***c*** and ***y*** fragments.

Effect of canonical nucleobases

As another difference between the CAD spectra of oppositely charged RNA ions, significantly increased backbone cleavage into ***c*** and ***y*** fragments on the 5′-side of adenosine residues was observed in CAD of $(M+nH)^{n+}$ but not $(M-nH)^{n-}$ ions, as illustrated in Figure 4 for RNA **3** (19 nt). Because positive charge facilitates backbone cleavage into ***c*** and ***y*** fragments, is it possible that preferred dissociation next to adenosine in CAD of $(M+nH)^{n+}$ ions is related to protonation? The proton affinities (PA) of A, C, G, and U nucleobases and nucleosides were evaluated to be 943, 950, 960, 873, and 989, 983, 993, 948 kJ/mol, respectively (49), with errors on the order of ±10 kJ/mol (50), indicating largely similar protonation probability for all bases except for U, which suggests that the observed effect of adenosine is not related to nucleobase protonation. The implicit conclusion that charge location does not significantly affect backbone cleavage into ***c*** and ***y*** fragments is further corroborated by fragment ion charge values, which indicate an intramolecular charge distribution according to simple Coulombic repulsion in largely extended $(M+4H)^{4+}$ and $(M-4H)^{4-}$ ion structures immediately before dissociation (Figure 5).

Increased backbone cleavage on the 5′-side of adenosine residues was also observed in CAD of $(M+nH)^{n+}$ ions of all other RNAs studied (Table 1). With increasing collision energy, however, the effect of adenosine on backbone cleavage decreased significantly (Figure 6). This suggests that preferred dissociation into ***c*** and ***y*** fragments next to A is based on structural elements that are not preserved at elevated internal energies.

In CAD $(M-nH)^{n-}$ ions, which generally required far higher energy (Figure 3A) than CAD of $(M+nH)^{n+}$ ions, somewhat increased backbone cleavage into ***c*** and ***y*** fragments on the 5′-side of guanosine residues was observed as illustrated in Figure 7 for RNA **1**. The factor by which cleavage next to G was increased compared to other residues in CAD of $(M-5H)^{5-}$ ions of RNA **1** decreased from 2.24 at 65 eV to 2.01 at 75 eV, similar to the trend shown in Figure 6 for the effect of A in CAD of $(M+4H)^{4+}$ ions. However, the effect of G appears to also depend on the RNA sequence

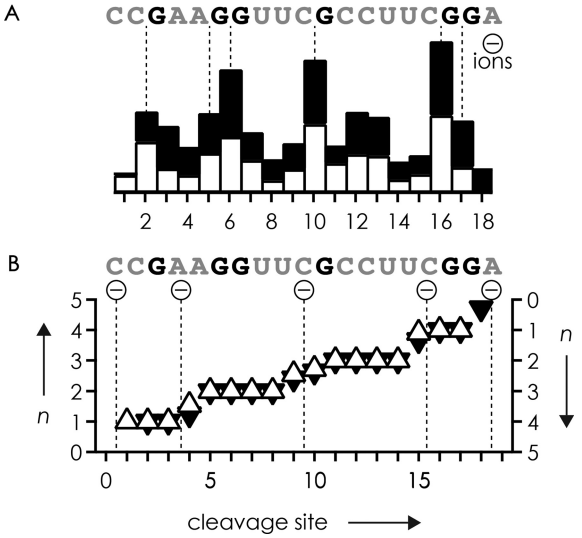

Figure 7. (**A**) relative abundances of ***c*** (black bars) and ***y*** (white bars) fragment ions from CAD of $(M\text{-}5H)^{5-}$ ions of RNA **1** versus cleavage site, using 65 eV laboratory frame collision energy; dashed lines highlight cleavage sites on the 5′-side of guanosine residues; (**B**) average charge *n* of ***c*** (filled triangles, left axis) and ***y*** (open triangles, right axis) fragment ions from CAD of $(M-5H)^{5-}$ ions of RNA **1** versus cleavage site using 65 eV laboratory frame collision energy; dashed lines indicate calculated charge locations.

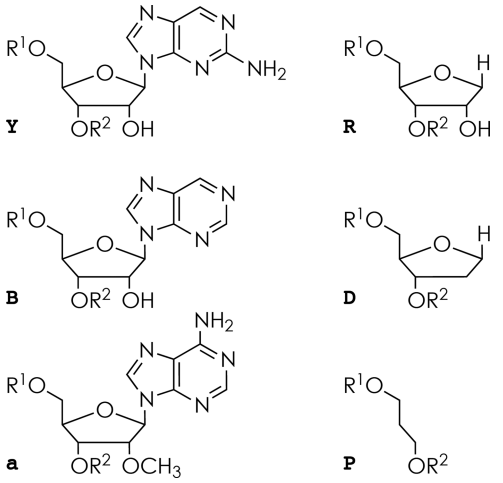

Scheme 2. Structures of nucleoside residues; Y: 2-aminopurine, B: nebularine, a: 2′-OCH_3 adenosine, R: ribose-spacer, D: 2′-deoxyribose-spacer, P: propanediol-linker.

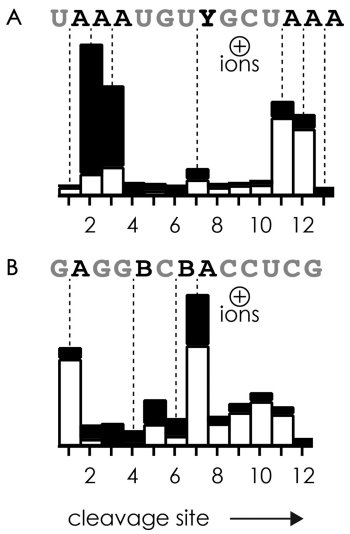

Figure 8. Relative abundances of ***c*** (black bars) and ***y*** (white bars) fragment ions from CAD of $(M+4H)^{4+}$ ions of (**A**) RNA **9** and (**B**) RNA **10** versus cleavage site, using (A) 48 eV and (B) 44 eV laboratory frame collision energies; dashed lines indicate backbone cleavage sites on the 5′-side of adenosine (A), nebularine (B), and 2-aminopurine (Y) residues.

as it was far less pronounced in CAD of $(M-5H)^{5-}$ ions of RNA **3** at 70 eV (Figure 4B). Nevertheless, the effects of G and A have in common that they show no correlation with the location of charge immediately before backbone cleavage (Figures 5 and 7) and that they decrease with increasing energy.

Effect of synthetic RNA modifications

While A can apparently form specific short-range interactions that facilitate phosphodiester bond cleavage in gaseous $(M+nH)^{n+}$ ions of RNA, the structurally related base 2-aminopurine (Y, Scheme 2) at position 6 of RNA **3** showed no appreciable effect on site-specific fragment ion abundance (Figure 4A). To further investigate this phenomenon, the $(M+4H)^{4+}$ ions of RNA **9** and **10** (Table 1) that comprise the bases nebularine (B, Scheme 2) and Y, respectively, were dissociated by CAD. As illustrated in Figure 8, neither B nor Y showed any effect on backbone cleavage that was comparable in magnitude to that of A.

Finally, the effects of selectively removing the ribose, its 2′-OH group, the nucleobase, and replacing the 2′-OH by 2′-OCH_3 were investigated. We found that the absence of a ribose 2′-OH group invariably inhibits backbone cleavage into ***c*** and ***y*** ions, as illustrated in Figure 9A–C for $(M+4H)^{4+}$ ions of 15 nt RNA (0.27 charges/nt) with D (**11**), P (**12**), and a (**14**) at sequence positions 6–9. Similar spectra without signals arising from ***c*** and ***y*** ions from cleavage at sites 6–9 were obtained by CAD of the corresponding $(M-4H)^{4-}$ ions at 64 eV laboratory frame energy (data not shown), in line with previous CAD studies of $(M-nH)^{n-}$ ions of RNA with 2′-OCH_3, 2′-F, and 2′-H modifications (17,22,37,40,51,52). CAD of more highly charged $(M-nH)^{n-}$ ions of RNA with 2′-modifications can nonetheless produce ***c*** and ***y*** ions at higher energies (along with ***a***, ***w***, ***b***, ***x***, ***d***, and/or ***w*** ions, Scheme 1) (40,53), for which a separate mechanism that solely involves the deprotonated phosphodiester moiety but not the adjoining nucleoside units has been proposed by Schürch *et al.* (51).

Surprisingly, CAD of $(M+4H)^{4+}$ ions of RNA with R at sequence positions 6–9 (**13**) produced increased yields of ***c*** and ***y*** fragments from cleavage at sites 6–9 (Figure 9D), suggesting that the nucleobase on the 3′-side of the phosphodiester bond may hinder nucleophilic attack of the ribose 2′-OH on the phosphorus by restricting the conformational flexibility of the ribose. However, the effect of R was not evident in CAD of $(M-4H)^{4-}$ ions of RNA **13** (Figure 9E), for which a laboratory frame energy of 64 eV was used in-

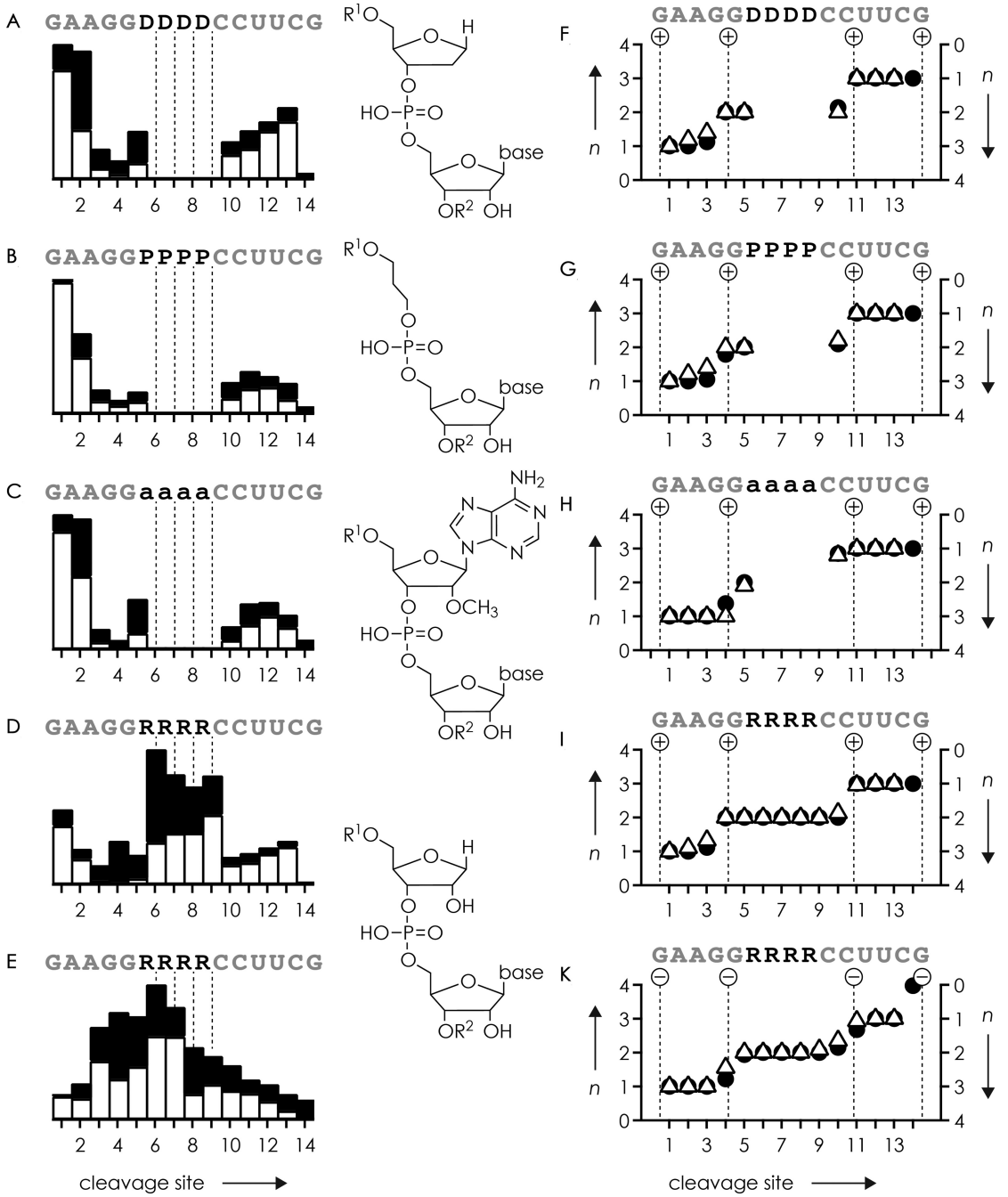

Figure 9. Relative abundances of ***c*** (black bars) and ***y*** (white bars) fragment ions from CAD of $(M+4H)^{4+}$ ions of RNA (**A**) **11**, (**B**) **12**, (**C**) **14**, (**D**) **13** at 44 eV laboratory frame collision energy and (**E**) $(M-4H)^{4-}$ ions of RNA **13** at 64 eV versus cleavage site; dashed lines indicate backbone cleavage sites on the 3′-side of D, P, a, and R residues; average charge *n* of ***c*** (circles, left axis) and ***y*** (triangles, right axis) fragment ions from CAD of $(M+4H)^{4+}$ ions of RNA (**F**) **11**, (**G**) **12**, (**H**) **14**, (**I**) **13** and (**K**) $(M-4H)^{4-}$ ions of RNA **13** versus cleavage site; dashed lines in (F)–(K) indicate calculated charge locations (see the supplementary material).

stead of the 44 eV for CAD of $(M+4H)^{4+}$ ions, suggesting that added energy restores ribose conformational flexibility.

Proton mobility and charge locations

As for the data in Figures 5 and 7, the charge values of fragments from CAD of RNA **11**, **12**, **13**, and **14** indicate intramolecular charge distributions according to simple Coulombic repulsion in largely extended ion structures immediately before dissociation, regardless of ion polarity, RNA composition, and whether or not backbone cleavage is observed at sites 6–9 (Figure 9). The ease with which both positive and negative charge distributes within vibrationally excited RNA $(M+nH)^{n+}$ and $(M-nH)^{n-}$ ions (Figures 5, 7, 9) reveals a high mobility of protons even in the absence of solvent, similar to that in peptide ions during CAD (35). At

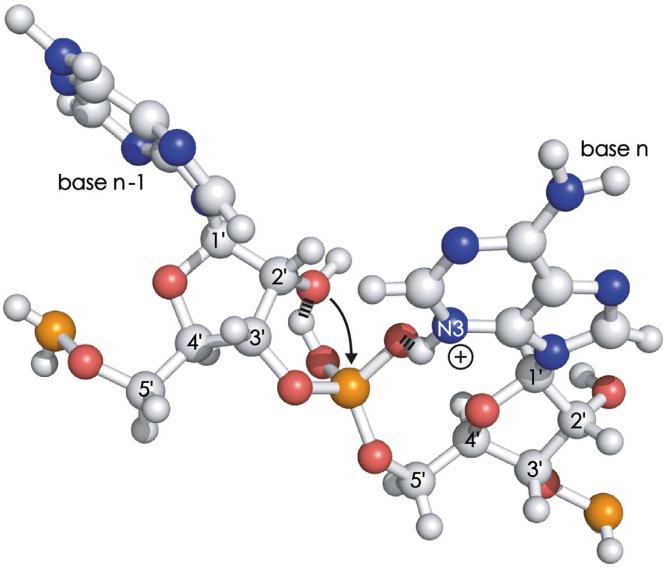

Scheme 3. Dinucleotide model (AA) illustrating a possible RNA structure in which nucleophilic attack of the 2′-OH group on the phosphorus (arrow) is facilitated by hydrogen bonding (dashed lines) between the phosphoric acid diester group and both the ribose and A (in *syn* conformation) protonated at N3.

the pH of ∼5 used here, extended RNA structures should carry a net negative charge in solution, i.e., should be deprotonated at all phosphodiester moieties and protonated at only a small fraction of the nucleobases A, C and G (54,55). However, depending on the polarity of the electrostatic potential applied to the emitter, ESI of the very same solution produced either $(M+nH)^{n+}$ or $(M-nH)^{n-}$ ions with net positive or negative charges whose abolute values were generally similar and far smaller than the number of phosphodiester moieties (Figure 1). This means that the number of charges, and therefore the sites where charge is located in gaseous RNA ions from ESI, are not the same as in solution, consistent with findings for smaller molecules (56) and a study of 22 nt RNA (57).

The high mobility of protons within vibrationally excited $(M+nH)^{n+}$ and $(M-nH)^{n-}$ ions, and the finding that charge is distributed according to Coulombic repulsion, is surprising in view of the proton affinities of A, C, G and U nucleobases (873–960 kJ/mol) (49) that differ by up to 87 kJ/mol; that of purine is 920 kJ/mol (49). RNAs **11**, **12** and **13** even lack any nucleobase at sequence positions 6–9, with RNA **12** also lacking the ribose (Figure 9). This implies that intramolecular proton transfer in vibrationally excited $(M+nH)^{n+}$ ions can also involve the phosphoric acid diester moiety, whose PA can be assumed to be close to that of phosphoric acid triethyl ester, 909 kJ/mol (49). Likewise, proton transfer in $(M\text{-}nH)^{n-}$ ions can proceed via both the phosphate diester groups (PA of dimethyl phosphate: ∼1380 kJ/mol) (49,58) and the deprotonated nucleobases A, C, G and U, for which PA values between 1406 and 1482 kJ/mol have been calculated (59–61).

Moreover, the proton affinities indicate that unlike in solution, the phosphodiester moieties of gaseous RNA $(M-nH)^{n-}$ and $(M+nH)^{n+}$ ions are not generally deprotonated. For the $(M-nH)^{n-}$ ions with 0.23 to 0.31 charges/nt studied here, deprotonation of all phosphodiester moieties would require that 69–77% of the nucleobases are protonated, which is highly unlikely as these percentages by far exceed the extent of base protonation in solution, and because the proton affinities of the nucleobases (873–960 kJ/mol) and the corresponding nucleosides (948–993 kJ/mol) (49) are substantially lower than the estimated PA of the deprotonated phosphodiester moiety (∼1380 kJ/mol). In other words, proton transfer from protonated nucleobases to deprotonated phosphodiester moieties in zwitterionic structures would be highly exothermic, with ΔH values between −387 and −507 kJ/mol. While intramolecular hydrogen bonding in the as yet unknown RNA ion structures can potentially alter the PAs of individual sites as discussed below, such effects are generally insufficient to turn the hypothetical proton transfer reaction from highly exothermic to endothermic (62). Consistent with these thermochemical considerations, a combined experimental and theoretical study showed that both neutral and deprotonated phosphodiester moieties are present in gaseous $(M-nH)^{n-}$ ions of 7 nt DNA with 0.29–0.57 charges/nt, along with negligible nucleobase protonation (63). Additional evidence for the non-zwitterionic nature of gaseous DNA ions came from a study of $(M-H)^{-}$ ions of dGTT, dTGT and dTTG (64). Moreover, the study of 7 nt DNA indicated that ionic hydrogen bonding between adjacent phosphodiester moieties allows for fast ($\leq 10^{-12}$ s) and reversible proton transfer without inducing any major changes in the gas phase structure of the ions such that protons can be dynamically shared by negatively charged phosphodiester moieties (63). In highly charged ions, however, all phosphodiester moieties can be deprotonated when their number equals the net negative charge of the ions as shown by photoelectron spectroscopy of $(M-nH)^{n-}$ ions of 3–5 nt DNA (65). Because none of the above characteristics of DNA directly concern the 2′-deoxyribose groups, similar behavior can be anticipated for gaseous $(M-nH)^{n-}$ ions of RNA. For the $(M+nH)^{n+}$ ions of RNA with 0.23–0.31 charges/nt studied here, deprotonation of all phosphodiester moieties would require that 69–77% and 23–31% of the nucleobases are singly and doubly protonated, respectively, which is even less likely than single base protonation in $(M-nH)^{n-}$ ions. This suggests that neither $(M-nH)^{n-}$ nor $(M+nH)^{n+}$ ions of RNA have zwitterionic structures in the gas phase, although in very large, gaseous noncovalent complexes of RNA (66,67), extensive hydrogen bonding networks could serve the role of solvent water in stabilizing oppositely charged sites.

DISCUSSION

The data from our study corroborate the hypothesis that the ribose 2′-OH group is critically involved in RNA backbone cleavage into ***c*** and ***y*** fragments by CAD (17,18,37,38), and we show here that this is the case for both $(M+nH)^{n+}$ and $(M-nH)^{n-}$ ions. The location of charge within vibrationally excited $(M+nH)^{n+}$ and $(M-nH)^{n-}$ ions immediately before dissociation, inferred from fragment ion charge values, showed no appreciable effect, which is strong evidence that phosphodiester bond cleavage does not directly involve charged sites. For CAD of $(M\text{-}nH)^{n-}$ ions, this conclusion is

in line with the earlier observation that more highly charged $(M-nH)^{n-}$ ions dissociate by a completely different mechanism that does not entail phosphodiester bond cleavage (39).

Importantly, the involvement of the ribose 2′-OH group shows that RNA dissociation into complementary ***c*** and ***y*** ions cannot be described as simple bond cleavage but instead proceeds via a more complex rearrangement reaction that apparently encompasses a sufficiently stable and long-lived intermediate state to allow time for proton redistribution prior to dissociation such that charge locations within RNA $(M+nH)^{n+}$ and $(M-nH)^{n-}$ ions immediately before phosphodiester bond cleavage can be different from those during nucleophilic attack of a ribose 2′-OH group on the adjacent phosphorus. The most reasonable intermediate structure is a cyclic pentacoordinate oxyphosphorane that has been implied in acid- and base-catalyzed RNA hydrolysis in solution (68–70), and in CAD of RNA $(M+H)^+$ and $(M-nH)^{n-}$ ions (17,38).

The multiple, low-energy collisions in CAD incrementally increase an ion's internal energy on a timescale of milliseconds to seconds (71). A stepwise reaction involving an intermediate state thus provides a rationale for the lack of any effect of observed charge locations on ***c*** and ***y*** ion yields (Figures 4, 5, 9), provided that the energy barrier for intramolecular proton transfer in gaseous RNA $(M+nH)^{n+}$ and $(M-nH)^{n-}$ ions is significantly lower than that for phosphodiester backbone cleavage. This means that positive and negative charges can facilitate and hinder nucleophilic attack at their initial locations in lower-energy RNA structures (70), respectively, but after formation of the intermediate, and before backbone cleavage, protons can move to new positions dictated by Coulomb repulsion in extended RNA structures.

Specifically, the above scenario provides a rationale for the effect of A in CAD of RNA $(M+nH)^{n+}$ ions. As illustrated in Scheme 3 for a dinucleotide model (AA), nucleophilic attack of the 2′-OH group on the phosphorus can be facilitated by hydrogen bonding between a nonbridging oxygen of the phosphoric acid diester group and A protonated at N3. Although N1 is the preferred site of protonation of adenine in the gas phase (59,72,73) and in solution (74), gaseous adenosine and adenosine monophosphate are preferentially protonated at N3 (75–80). This change in preferred site of protonation results from stabilization provided by intramolecular ionic hydrogen-bonding interactions (62), between N3 and O5′ in $(M+H)^+$ ions of both adenosine and 2′-deoxyadenosine (75), and between N3 and an oxygen of the phosphoric acid moiety in $(M+H)^+$ ions of 2′-deoxyadenosine and adenosine monophosphates (76–78,80). Nucleophilic attack can further be promoted by hydrogen bonding between the ribose 2′-OH group and the phosphodiester group (Scheme 3). Once a sufficiently stable intermediate structure, such as a cyclic pentacoordinate oxyphosphorane is formed, and the ion's internal energy is further increased, the RNA chain becomes more extended and protons can redistribute accordingly, after which even more added energy finally gives rise to phosphodiester backbone cleavage. A similar structure in which a neutral instead of a protonated base forms a hydrogen bond with a nonbridging oxygen of the phosphodiester group is conceivable for RNA $(M-nH)^{n-}$ ions. In support of this hypothesis, nucleobase–phosphate interactions have been identified in RNA crystals (81–83), and a recent study of RNA mononucleotide $(M-H)^-$ ions showed that the exocyclic amino group of G, in *syn* conformation, forms a hydrogen bond with the phosphate on the 5′-side, whereas A, C and U prefer the *anti* conformation that precludes such nucleobase-phosphate interactions (84).

The idea that local hydrogen bonding of protonated A and neutral G facilitates nucleophilic attack of the ribose 2′-OH group on the adjacent phosphorus is fully in line with experimental observations. First, the effects of A and G decreased with increasing energy, consistent with the disruption of hydrogen bonds at elevated energies. Second, the effect of G in CAD of $(M-nH)^{n-}$ ions, which required substantially higher energies than CAD of $(M+nH)^{n+}$ ions, was far less pronounced that the effect of A. Third, the identity of the nucleobase on the 5′-side of A (base $n-1$ in Scheme 3) does not appear to affect backbone cleavage (Figures 4A and 8), which suggests that the specific short-range interactions of A are limited to the adjacent phosphoric acid and ribose moieties.

The fact that among all of the bases studied in CAD of $(M+nH)^{n+}$ ions only A promoted backbone cleavage suggests that nucleobase proton affinities and their protonation sites in RNA $(M+nH)^{n+}$ ions are different from those of the free nucleobases as a result of local hydrogen bonding. Moreover, nucleobase properties other than proton affinity and hydrogen bonding capability, for example, their dipole moment, could also play a role. In general support of this hypothesis, computational chemistry calculations predict significantly different nucleobase dipole strengths and orientations for different RNA and related bases such as purine (59,85–89). The weak effect of G in CAD of $(M-nH)^{n-}$ ions could then be attributed to breaking of most hydrogen bonds at the elevated energies required for backbone cleavage, and to unfavorable hydrogen bonding patterns or weaker interactions of A, C, and U, which is strongly supported by the recent study of RNA mononucleotide $(M-H)^-$ ions mentioned above (84). In contrast to the effects of A and G on cleavage of the phosphodiester backbone bond on their 5′ side in CAD of RNA ions observed here, the transesterification and cleavage steps involved in RNA hydrolysis in solution are affected by both bases flanking the cleavage site (68,90,91). Moreover, nucleobase effects in solution were generally small (68,90) and rather nonsystematic (92), or even poorly reproducible, which was attributed to competing intra- and intermolecular interactions (93). Nevertheless, Linjalahti and Mikkolaa observed a significant increase in cleavage of the phosphodiester backbone bond on the 5′ side of A at neutral (5.5–7.5) but not at highly acidic (2) or basic (12) pH (93) and Li and Breaker found that cleavage on the 5′ side of G was somewhat increased at very high pH (∼14) (90). We plan to investigate this seemingly similar behavior in the gas and solution phases in future studies.

In conclusion, we have studied the dissociation of $(M-nH)^{n-}$ and $(M+nH)^{n+}$ ions of chemically modified and unmodified RNA by collisional activation, and found strong evidence for the formation of ***c*** and ***y*** fragment ions

by a stepwise mechanism similar to the transesterification and cleavage steps involved in RNA hydrolysis in solution (70). In the first step at lower ion internal energies, a pentacoordinate oxyphosphorane intermediate is formed by nucleophilic attack of a ribose 2′-OH group on the adjacent phosphorus. As observed here for adenine and guanine, nucleophilic attack can be facilitated by hydrogen bonding between the phosphodiester moiety and the adjacent nucleobase. In the next steps at elevated ion internal energies, the breaking of hydrogen bonds leads to extension of the RNA $(M-nH)^{n-}$ or $(M+nH)^{n+}$ ion structures and subsequent redistribution of charged sites according to simple Coulombic repulsion by intramolecular proton transfer, regardless of ion polarity, RNA composition, and whether or not backbone cleavage is observed. In the last step at even higher ion internal energies, the intermediate dissociates into ***c*** and complementary ***y*** fragments by cleavage of the phosphodiester backbone bond.

The energy barriers involved in dissociation of negatively charged RNA must be substantially higher than those for positively charged RNA, as CAD of $(M-nH)^{n-}$ ions required far higher energies than CAD of $(M+nH)^{n+}$ ions. Moreover, in CAD of both $(M+nH)^{n+}$ and $(M-nH)^{n-}$ ions, the energy barriers for each step can be ranked as: nucleophilic attack to form intermediate < breaking of hydrogen bonds and extension of RNA structure < intramolecular proton transfer < phosphodiester bond cleavage into ***c*** and ***y*** fragments.

The detailed new insights into the mechanism of RNA $(M+nH)^{n+}$ and $(M-nH)^{n-}$ ion dissociation by CAD reported here provide a solid basis for future mechanistic studies. Specifically, if the apparent similarity of phosphodiester bond cleavage in solution and the gas phase can be further substantiated, gaseous RNA can serve as a valid model for the investigation of the effect of metal ions and other adducts on the transesterification and cleavage steps involved in (enzymatic) RNA hydrolysis in solution. For RNA sequencing applications and top-down MS studies that rely on site-specific, relative fragment ion abundances for the relative quantitation of synthetic or posttranscriptional modifications (28), CAD of $(M-nH)^{n-}$ ions offers the advantages of higher ion yields and more random phosphodiester bond cleavage. CAD of $(M+nH)^{n+}$ ions, on the other hand, requires significantly lower energies and thus may be more useful for the characterization of RNA carrying labile modifications.

SUPPLEMENTARY DATA

Supplementary Data are available at NAR Online.

FUNDING

Austrian Science Fund (FWF) [Y372 and P27347 to K.B., I1040 and P21641 to R.M.]; National Science Foundation [OISE-0730072 and CHE-1409420 to M.T.R.]. Funding for open access charge: FWF.
Conflict of interest statement. None declared.

REFERENCES

1. Hüttenhofer,A., Schattner,P. and Polacek,N. (2005) Non-coding RNAs: hope or hype? *Trends Genet.*, **21**, 289–297.
2. Eddy,S.R. (2001) Non-coding RNA genes and the modern RNA world. *Nat. Rev. Genet.*, **2**, 919–929.
3. Wang,X. and He,C. (2014) Dynamic RNA modifications in posttranscriptional regulation. *Mol. Cell*, **56**, 5–12.
4. Helm,M. and Alfonzo,J.D. (2014) Posttranscriptional RNA modifications: playing metabolic games in a cell's chemical Legoland. *Chem. Biol.*, **21**, 174–185.
5. Amort,T., Souliere,M.F., Wille,A., Jia,X.Y., Fiegl,H., Wörle,H., Micura,R. and Lusser,A. (2013) Long non-coding RNAs as targets for cytosine methylation. *RNA Biol.*, **10**, 1003–1009.
6. Kellner,S., Burhenne,J. and Helm,M. (2010) Detection of RNA modifications. *RNA Biol.*, **7**, 237–247.
7. Kellner,S., Ochel,A., Thuring,K., Spenkuch,F., Neumann,J., Sharma,S., Entian,K.D., Schneider,D. and Helm,M. (2014) Absolute and relative quantification of RNA modifications via biosynthetic isotopomers. *Nucleic Acids Res.*, **42**, e142.
8. Brandmayr,C., Wagner,M., Bruckl,T., Globisch,D., Pearson,D., Kneuttinger,A.C., Reiter,V., Hienzsch,A., Koch,S., Thoma,I. *et al.* (2012) Isotope-based analysis of modified tRNA nucleosides correlates modification density with translational efficiency. *Angew. Chem.*, **51**, 11162–11165.
9. Liu,N., Parisien,M., Dai,Q., Zheng,G., He,C. and Pan,T. (2013) Probing N6-methyladenosine RNA modification status at single nucleotide resolution in mRNA and long noncoding RNA. *RNA*, **19**, 1848–1856.
10. Schaefer,M., Pollex,T., Hanna,K. and Lyko,F. (2009) RNA cytosine methylation analysis by bisulfite sequencing. *Nucleic Acids Res.*, **37**, e12.
11. Wang,B.H. and Biemann,K. (1994) Matrix-assisted laser desorption/ionization time-of-flight mass spectrometry of chemically modified oligonucleotides. *Anal. Chem.*, **66**, 1918–1924.
12. Limbach,P.A. (1996) Indirect mass spectrometric methods for characterizing and sequencing oligonucleotides. *Mass Spectrom. Rev.*, **15**, 297–336.
13. Hahner,S., Lüdemann,H.C., Kirpekar,F., Nordhoff,E., Roepstorff,P., Galla,H.J. and Hillenkamp,F. (1997) Matrix-assisted laser desorption/ionization mass spectrometry (MALDI) of endonuclease digests of RNA. *Nucleic Acids Res.*, **25**, 1957–1964.
14. Noon,K.R., Bruenger,E. and McCloskey,J.A. (1998) Posttranscriptional modifications in 16S and 23S rRNAs of the archaeal hyperthermophile Sulfolobus solfataricus. *J. Bacteriol.*, **180**, 2883–2888.
15. Polo,L.M. and Limbach,P.A. (1998) Matrix-assisted laser desorption/ionization time-of-flight mass spectrometry for the analysis of RNase H cleavage products. *J. Mass Spectrom.*, **33**, 1226–1231.
16. Yu,E. and Fabris,D. (2003) Direct probing of RNA structures and RNA-protein interactions in the HIV-1 packaging signal by chemical modification and electrospray ionization fourier transform mass spectrometry. *J. Mol. Biol.*, **330**, 211–223.
17. Tromp,J.M. and Schürch,S. (2005) Gas-phase dissociation of oligoribonucleotides and their analogs studied by electrospray ionization tandem mass spectrometry. *J. Am. Soc. Mass Spectrom.*, **16**, 1262–1268.
18. Tromp,J.M. and Schürch,S. (2006) Electrospray ionization tandem mass spectrometry of biphenyl-modified oligo(deoxy)ribonucleotides. *Rapid Commun. Mass Spectrom.*, **20**, 2348–2354.
19. Turner,K.B., Hagan,N.A., Kohlway,A.S. and Fabris,D. (2006) Mapping noncovalent ligand binding to stemloop domains of the HIV-1 packaging signal by tandem mass spectrometry. *J. Am. Soc. Mass Spectrom.*, **17**, 1401–1411.
20. Douthwaite,S. and Kirpekar,F. (2007) Identifying modifications in RNA by MALDI mass spectrometry. *Methods Enzymol.*, **425**, 3–20.
21. Emmerechts,G., Maes,L., Herdewijn,P., Anne,J. and Rozenski,J. (2008) Characterization of the posttranscriptional modifications in Legionella pneumophila small-subunit ribosomal RNA. *Chem. Biodivers.*, **5**, 2640–2653.

22. Bahr,U., Aygun,H. and Karas,M. (2009) Sequencing of single and double stranded RNA oligonucleotides by acid hydrolysis and MALDI mass spectrometry. *Anal. Chem.*, **81**, 3173–3179.
23. Taucher,M. and Breuker,K. (2010) Top-down mass spectrometry for sequencing of larger (up to 61 nt) RNA by CAD and EDD. *J. Am. Soc. Mass Spectrom.*, **21**, 918–929.
24. Taucher,M., Rieder,U. and Breuker,K. (2010) Minimizing base loss and internal fragmentation in collisionally activated dissociation of multiply deprotonated RNA. *J. Am. Soc. Mass Spectrom.*, **21**, 278–285.
25. Huang,T.Y., Liu,J.A. and McLuckey,S.A. (2010) Top-down tandem mass spectrometry of tRNA via ion trap collision-induced dissociation. *J. Am. Soc. Mass Spectrom.*, **21**, 890–898.
26. Taucher,M., Ganisl,B. and Breuker,K. (2011) Identification, localization, and relative quantitation of pseudouridine in RNA by tandem mass spectrometry of hydrolysis products. *Int. J. Mass Spectrom.*, **304**, 91–97.
27. Taucher,M. and Breuker,K. (2012) Characterization of modified RNA by top-down mass spectrometry. *Angew. Chem.*, **51**, 11289–11292.
28. Micura,R., Kreutz,C. and Breuker,K. (2013) A personal perspective on chemistry-driven RNA research. *Biopolymers*, **99**, 1114–1123.
29. Fisher,H.C., Smith,M. and Ashcroft,A.E. (2013) De novo sequencing of short interfering ribonucleic acids facilitated by use of tandem mass spectrometry with ion mobility spectrometry. *Rapid Commun. Mass Spectrom.*, **27**, 2247–2254.
30. Limbach,P.A., Crain,P.F. and McCloskey,J.A. (1995) Molecular mass measurement of intact ribonucleic acids via electrospray ionization quadrupole mass spectrometry. *J. Am. Soc. Mass Spectrom.*, **6**, 27–39.
31. Sannes-Lowery,K.A., Hu,P.F., Mack,D.P., Mei,H.Y. and Loo,J.A. (1997) HIV 1 Tat peptide binding to TAR RNA by electrospray ionization mass spectrometry. *Anal. Chem.*, **69**, 5130–5135.
32. Hofstadler,S.A., Griffey,R.H., Pasa-Tolic,L. and Smith,R.D. (1998) The use of a stable internal mass standard for accurate mass measurements of oligonucleotide fragment ions using electrospray ionization Fourier transform ion cyclotron resonance mass spectrometry with infrared multiphoton dissociation. *Rapid Commun. Mass Spectrom.*, **12**, 1400–1404.
33. Sannes-Lowery,K.A., Mack,D.P., Hu,P.F., Mei,H.Y. and Loo,J.A. (1997) Positive ion electrospray ionization mass spectrometry of oligonucleotides. *J. Am. Soc. Mass Spectrom.*, **8**, 90–95.
34. Laskin,J. and Futrell,J.H. (2003) Collisional activation of peptide ions in FT-ICR mass spectrometry. *Mass Spectrom. Rev.*, **22**, 158–181.
35. Dongre,A.R., Jones,J.L., Somogyi,A. and Wysocki,V.H. (1996) Influence of peptide composition, gas-phase basicity, and chemical modification on fragmentation efficiency: evidence for the mobile proton model. *J. Am. Chem. Soc.*, **118**, 8365–8374.
36. Kirpekar,F. and Krogh,T.N. (2001) RNA fragmentation studied in a matrix-assisted laser desorption/ionisation tandem quadrupole/orthogonal time-of-flight mass spectrometer. *Rapid Commun. Mass Spectrom.*, **15**, 8–14.
37. Schürch,S., Bernal-Mendez,E. and Leumann,C.J. (2002) Electrospray tandem mass spectrometry of mixed-sequence RNA/DNA oligonucleotides. *J. Am. Soc. Mass Spectrom.*, **13**, 936–945.
38. Andersen,T.E., Kirpekar,F. and Haselmann,K.F. (2006) RNA fragmentation in MALDI mass spectrometry studied by H/D-exchange: mechanisms of general applicability to nucleic acids. *J. Am. Soc. Mass Spectrom.*, **17**, 1353–1368.
39. Huang,T.Y., Kharlamova,A., Liu,J. and McLuckey,S.A. (2008) Ion trap collision-induced dissociation of multiply deprotonated RNA: ***c***/***y***-Ions versus (***a***-B)/***w***-ions. *J. Am. Soc. Mass Spectrom.*, **19**, 1832–1840.
40. Gao,Y. and McLuckey,S.A. (2012) Collision-induced dissociation of oligonucleotide anions fully modified at the 2′-position of the ribose: 2′-F/-H and 2′-F/-H/-OMe mix-mers. *J. Mass Spectrom.*, **47**, 364–369.
41. Gardner,M.W., Li,N., Ellington,A.D. and Brodbelt,J.S. (2010) Infrared multiphoton dissociation of small-interfering RNA anions and cations. *J. Am. Soc. Mass Spectrom.*, **21**, 580–591.
42. Hanwell,M.D., Curtis,D.E., Lonie,D.C., Vandermeersch,T., Zurek,E. and Hutchison,G.R. (2012) Avogadro: an advanced semantic chemical editor, visualization, and analysis platform. *J. Cheminform.*, **4**, 17.
43. Pitsch,S., Weiss,P.A., Jenny,L., Stutz,A. and Wu,X.L. (2001) Reliable chemical synthesis of oligoribonucleotides (RNA) with 2′-O-[(triisopropylsilyl)oxy]methyl(2′-O-tom)-protected phosphoramidites. *Helv. Chim. Acta*, **84**, 3773–3795.
44. Micura,R. (2002) Small interfering RNAs and their chemical synthesis. *Angew. Chem.*, **41**, 2265–2269.
45. Pils,W. and Micura,R. (2000) Flexible non-nucleotide linkers as loop replacements in short double helical RNAs. *Nucleic Acids Res.*, **28**, 1859–1863.
46. Wawrzyniak-Turek,K. and Höbartner,C. (2014) Enzymatic combinatorial nucleoside deletion scanning mutagenesis of functional RNA. *Chem. Commun.*, **50**, 10937–10940.
47. Huang,T.Y., Liu,J., Liang,X.R., Hodges,B.D.M. and McLuckey,S.A. (2008) Collision-induced dissociation of intact duplex and single-stranded siRNA anions. *Anal. Chem.*, **80**, 8501–8508.
48. McLuckey,S.A., Van Berkel,G.J. and Glish,G.L. (1992) Tandem mass-spectrometry of small, multiply charged oligonucleotides. *J. Am. Soc. Mass Spectrom.*, **3**, 60–70.
49. NIST Chemistry WebBook. In: Linstrom,PJ and Mallard,WG (eds). *NIST Standard Reference Database Number*. 69.
50. Meot-Ner,M. (2003) The proton affinity scale, and effects of ion structure and solvation. *Int. J. Mass Spectrom.*, **227**, 525–554.
51. Nyakas,A., Stucki,S.R. and Schürch,S. (2011) Tandem mass spectrometry of modified and platinated oligoribonucleotides. *J. Am. Soc. Mass Spectrom.*, **22**, 875–887.
52. Smith,S.I. and Brodbelt,J.S. (2011) Hybrid activation methods for elucidating nucleic acid modifications. *Anal. Chem.*, **83**, 303–310.
53. Gao,Y., Yang,J., Cancilla,M.T., Meng,F.Y. and McLuckey,S.A. (2013) Top-down interrogation of chemically modified oligonucleotides by negative electron transfer and collision induced dissociation. *Anal. Chem.*, **85**, 4713–4720.
54. Verdolino,V., Cammi,R., Munk,B.H. and Schlegel,H.B. (2008) Calculation of pK(a) Values of nucleobases and the guanine oxidation products guanidinohydantoin and spiroiminodihydantoin using density functional theory and a polarizable continuum model. *J. Phys. Chem. B*, **112**, 16860–16873.
55. Acharya,P., Cheruku,P., Chatterjee,S., Acharya,S. and Chattopadhyaya,J. (2004) Measurement of nucleobase pK(a) values in model mononucleotides shows RNA-RNA duplexes to be more stable than DNA-DNA duplexes. *J. Am. Chem. Soc.*, **126**, 2862–2869.
56. Chang,T.M., Prell,J.S., Warrick,E.R. and Williams,E.R. (2012) Where's the charge? Protonation sites in gaseous ions change with hydration. *J. Am. Chem. Soc.*, **134**, 15805–15813.
57. Ganisl,B., Taucher,M., Riml,C. and Breuker,K. (2011) Charge as you like! Efficient manipulation of negative ion net charge in electrospray ionization of proteins and nucleic acids. *Eur. J. Mass Spectrom.*, **17**, 333–343.
58. Moser,A., Range,K. and York,D.M. (2010) Accurate proton affinity and gas-phase basicity values for molecules important in biocatalysis. *J. Phys. Chem. B*, **114**, 13911–13921.
59. Zhachkina,A., Liu,M., Sun,X.J., Amegayibor,F.S. and Lee,J.K. (2009) Gas-phase thermochemical properties of the damaged base O(6)-methylguanine versus adenine and guanine. *J. Org. Chem.*, **74**, 7429–7440.
60. Liu,M., Li,T.T., Amegayibor,F.S., Cardoso,D.S., Fu,Y.L. and Lee,J.K. (2008) Gas-phase thermochemical properties of pyrimidine nucleobases. *J. Org. Chem.*, **73**, 9283–9291.
61. Kurinovich,M.A. and Lee,J.K. (2002) The acidity of uracil and uracil analogs in the gas phase: four surprisingly acidic sites and biological implications. *J. Am. Soc. Mass Spectrom.*, **13**, 985–995.
62. Meot-Ner,M. (2005) The ionic hydrogen bond. *Chem. Rev.*, **105**, 213–284.
63. Arcella,A., Dreyer,J., Ippoliti,E., Ivani,I., Portella,G., Gabelica,V., Carloni,P. and Orozco,M. (2015) Structure and dynamics of oligonucleotides in the gas phase. *Angew. Chem.*, **54**, 467–471.
64. Gidden,J. and Bowers,M.T. (2003) Gas-phase conformations of deprotonated trinucleotides (dGTT(-), dTGT(-), and dTTG(-)): The question of zwitterion formation. *J. Am. Soc. Mass Spectrom.*, **14**, 161–170.
65. Vonderach,M., Ehrler,O.T., Matheis,K., Weis,P. and Kappes,M.M. (2012) Isomer-selected photoelectron spectroscopy of isolated DNA

oligonucleotides: phosphate and nucleobase deprotonation at high negative charge states. *J. Am. Chem. Soc.*, **134**, 7830–7841.
66. Rostom,A.A., Fucini,P., Benjamin,D.R., Juenemann,R., Nierhaus,K.H., Hartl,F.U., Dobson,C.M. and Robinson,C.V. (2000) Detection and selective dissociation of intact ribosomes in a mass spectrometer. *Proc. Natl. Acad. Sci. U.S.A.*, **97**, 5185–5190.
67. Hofstadler,S.A. and Griffey,R.H. (2001) Analysis of noncovalent complexes of DNA and RNA by mass spectrometry. *Chem. Rev.*, **101**, 377–390.
68. Oivanen,M., Kuusela,S. and Lonnberg,H. (1998) Kinetics and mechanisms for the cleavage and isomerization of the phosphodiester bonds of RNA by Bronsted acids and bases. *Chem. Rev.*, **98**, 961–990.
69. Kellerman,D.L., York,D.M., Piccirilli,J.A. and Harris,M.E. (2014) Altered (transition) states: mechanisms of solution and enzyme catalyzed RNA 2′-O-transphosphorylation. *Curr. Opin. Chem. Biol.*, **21**, 96–102.
70. Perreault,D.M. and Anslyn,E.V. (1997) Unifying the current data on the mechanism of cleavage – transesterification of RNA. *Angew. Chem.*, **36**, 432–450.
71. McLuckey,S.A. and Goeringer,D.E. (1997) Slow heating methods in tandem mass spectrometry. *J. Mass Spectrom.*, **32**, 461–474.
72. Russo,N., Toscano,M., Grand,A. and Jolibois,F. (1998) Protonation of thymine, cytosine, adenine, and guanine DNA nucleic acid bases: theoretical investigation into the framework of density functional theory. *J. Comput. Chem.*, **19**, 989–1000.
73. Turecek,F. and Chen,X.H. (2005) Protonated adenine: tautomers, solvated clusters, and dissociation mechanisms. *J. Am. Soc. Mass Spectrom.*, **16**, 1713–1726.
74. Kapinos,L.E., Operschall,B.P., Larsen,E. and Sigel,H. (2011) Understanding the acid-base properties of adenosine: the intrinsic basicities of N1, N3 and N7. *Chem. Eur. J.*, **17**, 8156–8164.
75. Wu,R., Yang,B., Berden,G., Oomens,J. and Rodgers,M.T. (2015) Gas-phase conformations and energetics of protonated 2′-deoxyadenosine and adenosine: IRMPD action spectroscopy and theoretical studies. *J. Phys. Chem. B*, **119**, 2795–2805.
76. Gidden,J. and Bowers,M.T. (2003) Gas-phase conformations of deprotonated and protonated mononucleotides determined by ion mobility and theoretical modeling. *J. Phys. Chem. B*, **107**, 12829–12837.
77. Green-Church,K.B. and Limbach,P.A. (2000) Mononucleotide gas-phase proton affinities as determined by the kinetic method. *J. Am. Soc. Mass Spectrom.*, **11**, 24–32.
78. Green-Church,K.B., Limbach,P.A., Freitas,M.A. and Marshall,A.G. (2001) Gas-phase hydrogen/deuterium exchange of positively charged mononucleotides by use of Fourier-transform ion cyclotron resonance mass spectrometry. *J. Am. Soc. Mass Spectrom.*, **12**, 268–277.
79. Touboul,D., Bouchoux,G. and Zenobi,R. (2008) Gas-phase protonation thermochemistry of adenosine. *J. Phys. Chem. B*, **112**, 11716–11725.
80. Milosavljevic,A.R., Cerovski,V.Z., Canon,F., Rankovic,M.L., Skoro,N., Nahon,L. and Giuliani,A. (2014) Energy-dependent UV photodissociation of gas-phase adenosine monophosphate nucleotide ions: the role of a single solvent molecule. *J. Phys. Chem. Lett.*, **5**, 1994–1999.
81. Zirbel,C.L., Sponer,J.E., Sponer,J., Stombaugh,J. and Leontis,N.B. (2009) Classification and energetics of the base-phosphate interactions in RNA. *Nucleic Acids Res.*, **37**, 4898–4918.
82. Ulyanov,N.B. and James,T.L. (2010) RNA structural motifs that entail hydrogen bonds involving sugar-phosphate backbone atoms of RNA. *New J. Chem.*, **34**, 910–917.
83. Sheng,J., Zhang,W., Hassan,A.E.A., Gan,J.H., Soares,A.S., Geng,S., Ren,Y. and Huang,Z. (2012) Hydrogen bond formation between the naturally modified nucleobase and phosphate backbone. *Nucleic Acids Res.*, **40**, 8111–8118.
84. Nei,Y.W., Crampton,K.T., Berden,G., Oomens,J. and Rodgers,M.T. (2013) Infrared multiple photon dissociation action spectroscopy of deprotonated RNA mononucleotides: gas-phase conformations and energetics. *J. Phys. Chem. A*, **117**, 10634–10649.
85. Rodgers,M.T. and Armentrout,P.B. (2000) Noncovalent interactions of nucleic acid bases (uracil, thymine, and adenine) with alkali metal ions. Threshold collision-induced dissociation and theoretical studies. *J. Am. Chem. Soc.*, **122**, 8548–8558.
86. Sponer,J., Leszczynski,J. and Hobza,P. (2001) Electronic properties, hydrogen bonding, stacking, and cation binding of DNA and RNA bases. *Biopolymers*, **61**, 3–31.
87. Kostko,O., Bravaya,K., Krylov,A. and Ahmed,M. (2010) Ionization of cytosine monomer and dimer studied by VUV photoionization and electronic structure calculations. *Phys. Chem. Chem. Phys.*, **12**, 2860–2872.
88. Alparone,A. (2013) Linear and nonlinear optical properties of nucleic acid bases. *Chem. Phys.*, **410**, 90–98.
89. Sharma,S. and Lee,J.K. (2004) Gas-phase acidity studies of multiple sites of adenine and adenine derivatives. *J. Org. Chem.*, **69**, 7018–7025.
90. Li,Y.F. and Breaker,R.R. (1999) Kinetics of RNA degradation by specific base catalysis of transesterification involving the 2′-hydroxyl group. *J. Am. Chem. Soc.*, **121**, 5364–5372.
91. Witzel,H. (1960) Einfluss der Nucleotidbasen auf die nicht-enzymatische Spaltung der Ribonucleinsäure-Diester-Bindungen. *Liebigs Ann. Chem.*, **635**, 182–191.
92. Jarvinen,P., Oivanen,M. and Lonnberg,H. (1991) Interconversion and phosphoester hydrolysis of 2′,5′-dinucleoside and 3′,5′-dinucleoside monophosphates – kinetics and mechanisms. *J. Org. Chem.*, **56**, 5396–5401.
93. Linjalahti,H. and Mikkola,S. (2007) Intra- and intermolecular interactions influence the reactivity of RNA oligonucleotides. *Chem. Biodivers.*, **4**, 2938–2947.